Tissue and Tumor Epithelium Classification using Fine-tuned Deep CNN Models

Anju T E[1]
Research Scholar, Dept. of Computer Science
Mother Teresa Women's University
Kodaikanal, India

Dr. S. Vimala[2]
Associate Professor, Dept. of Computer Science
Mother Teresa Women's University
Kodaikanal, India

***Abstract*—The field of Digital Pathology (DP) has become more interested in automated tissue phenotyping in recent years. Tissue phenotyping may be used to identify colorectal cancer (CRC) and distinguish various cancer types. The information needed to construct automated tissue phenotyping systems has been made available by the introduction of Whole Slide Images (WSIs). One of the typical pathological diagnosis duties for pathologists is the histopathological categorization of epithelial tumors. Artificial intelligence (AI) based computational pathology approaches would be extremely helpful in reducing the pathologists ever-increasing workloads, particularly in areas where access to pathological diagnosis services is limited. Investigating several deep learning models for categorizing the images of tumor epithelium from histology is the initial goal. The varying accuracy ratings that were achieved for the deep learning models on the same database demonstrated that additional elements like pre-processing, data augmentation, and transfer learning techniques might affect the models' capacity to attain better accuracy. The second goal of this publication is to reduce the time taken to classify the tissue and tumor Epithelium. The final goal is to examine and fine-tune the most recent models that have received little to no attention in earlier research. These models were checked by the histology Kather CRC image database's nine classifications (CRC-VAL-HE-7K, NCT-CRC-HE-100K). To identify and recommend the most cutting-edge models for each categorization, these models were contrasted with those from earlier research. The performance and the achievements of the proposed preprocessing workflow and fine-tuned Deep CNN models (Alexnet, GoogLeNet and Inceptionv3) are greater compared to the prevalent methods.**

***Keywords*—Colorectal cancer; deep learning; CNN; tumor epithelium; Alexnet; GoogLeNet; Inceptionv3**

I. INTRODUCTION

Historically, pathologists have examined the micro-anatomy of cells and tissues under a microscope. The development of Digital Pathology (DP) imaging in recent years has given pathologists an alternative method to perform the same analysis on a computer screen [1]. The current inquiry methodologies for breast cancer include mammography, magnetic resonance imaging (MRI), and pathology examinations. The histopathological scans are recognized as a golden standard to improve the diagnostic accuracy for patients who also had other investigations, such as mammography [2]. Additionally, a histopathological examination can offer more thorough and trustworthy information to detect cancer and to evaluate, how it affects the tissues around it [3]–[5]. The new modality, digital pathology imaging, now makes WSI (Whole Slide Imaging) a reality. Through WSI, the images may be shared, viewed on a digital display, and can be controlled/ examined on a screen [6]. Tumor architecture in Colorectal Cancer (CRC) evolves as the disease progresses [7] and is associated with patient prognosis [8]. Therefore, it is important for histopathologists to quantify the tissue composition in CRC. Inter-tumor heterogeneity and intra-tumor heterogeneity are both forms of tumor heterogeneity. By the different signals that cells pick up from their microenvironment, the tumor microenvironment (TME) really plays a significant role in the establishment of intra-tumor heterogeneity (ITH) [9]. The third most common cancer type to cause mortality is colorectal cancer (CRC), which is ranked as the fourth most common cancer [10]. In fact, treating patients and saving their lives depends on early-stage CRC diagnosis [11]. For the classification and prognostication of cancer, the study of tumor heterogeneity is crucial [12]. In-tumor heterogeneity can help to clarify, how TME affects patient prognosis and can also be used to spot new aggressive phenotypes that may be potential targets for future therapies [13]. Although most present histological analysis relies on the pathologists' subjective assessments, a critical need for automating the various processing techniques arises, that can provide good quantitative analysis and throughput of the digital pathology images for precise identification and assessment of various tumor epitheliums.

Deep convolutional neural networks (CNNs) algorithms automatically analyse images for handling classification and detection tasks, reducing the amount of manual labour necessary for the feature-extraction operations [14]. The lack of a suitably sizable annotated data set for training is a significant barrier to applying deep learning to many biological domains. Transfer learning, which makes use of deep CNNs that have already been trained on a significant amount of natural scene data, may be used to circumvent the need for sample size, nevertheless. This approach is based on the notion that the characteristics discovered by deep CNNs to identify classes in a dataset may also be useful for clinical data sets with marginally worse performance.

In medical domain there are currently three approaches in deep learning: (i). Acquiring features learned in the training phase of deep CNN with numerous natural images, then the features acquired are used for classifier training [15], [16], and [17], (ii) fine-tuning a small number of network layers are fine tuned in the pre-trained CNN on a desired data set [18], (iii)

training directly the deep CNN with real-world data. The author in [19] suggests categorizing brain tumor based on multiphase MRI scans and compares the outcomes to several deep learning structure configurations and baseline neural networks.

Based on the findings of this work, the effectiveness of identifying tumor epithelial tissues using transfer learning approaches in the area: In what ways, would fine-tuning the models in the Validation Frequency, Dropout Layer, and Classification Layer improve the classification performance, were investigated.

II. Related Works

The classification of the different tissue types in histological images is frequently done under supervision [20]. Modern approaches for phenotyping CRC tissues under supervision can be divided into two groups: learnt methods [23,24] and methods based on texture [21]. Additionally, other efforts, like [24], integrated shallow and deep characteristics. In order to extract certain structures from image areas, hand-crafted techniques known as "texture approaches" were developed [25]. Deep learning techniques, on the other hand, have the capacity to directly learn more pertinent and sophisticated image characteristics across layers, particularly, when the relationship between both the source data as well as the expected outcomes is not known in advance. As pathological imaging activities are incredibly complex and there is little knowledge on which quantitative image properties predict the outcomes, deep learning approaches are suitable for these activities [26, 27]. In [20], Kather et al. did the primary researches to handle CRC multi-class tissue types where 5000 histological pictures were used to create a database that included eight different CRC types of tissues. Modern texture descriptors and classifiers were put to the test by J. N. Kather and colleagues. Their suggested strategy is based on a promising mix of global lower-order texture metrics along with local descriptors from GLCM and LBP. The General Purpose (GenP) approach, which Nanni et al. proposed in [24], is based on the collection of learned features, hand-crafted, and dense sampling. In their proposed method, all features were trained using SVM, and the integration were achieved using the sum rule. To differentiate between the various CRC tissue types, [28] evaluated shallow and deep characteristics. In their research, they looked at how dimensionality reduction techniques affected accuracy and computing expense. Their findings demonstrated that CNN-based features may achieve the best accuracy/dimensionality trade-off. In [29], J. N. Kather et al. created a dataset consisting of one lakh images which categorized eight tissue types using eighty-six H&E slides of CRC tissues. They evaluated the AlexNet [31,38], ResNet-50 [34], GoogLeNet [33], VGG19 [30], and SqueezeNet version-1.1 [32] pretrained CNN models. They came to the conclusion that among the five CNN models, VGG19 was the best. A novel CRC-TP database with 280K patches taken from 20 WSIs of CRC and divided into seven different tissue phenotypes was proposed by Javed et al. [22]. They employed 27 cutting-edge techniques, including texture, CNN, and Graph CNN-based approaches (GCN), to categorize different tissue types. According to their test findings, the GCN performed better than the texturing and CNN approaches. Although hand-crafted feature-based and deep learning approaches have been employed to classify many CRC tissue types, their performance still needs to be enhanced. In order to do this, deep CNN methods have been enhanced that significantly outperformed baseline results on two well-known databases.

III. Materials and Methods

A. Kather-CRC-Data set

This dataset contains non-overlapping 100,000 image patches, which include histological images of healthy tissue and CRC in humans (H&E). Each image is 224x224 pixels (px), with a pixel size of 0.5 microns (MPP). Adipose tissue, background (no tissue), detritus, lymphocytes, normal mucosa, mucus, stroma, muscle, and tumor epithelium were the nine types of tissues that were chosen from their database. The NCT Biobank and the UMM Pathology Archive provided the 86 formalin-fixed paraffin-embedded (FFPE) samples from which these images were manually retrieved. The tissue samples included CRC original tumor slides and tumor tissue from CRC liver metastases. To improve variety, non-tumorous gastrectomy specimen sections were included to the normal tissue classes.

Five samples of each CRC tissue type are shown in Fig. 2 from the Kather-CRC-NCT-CRC-HE-100K database. Tenfold cross validation was performed by J. N. Kather et al. [12] (http://dx.doi.org/10.5281/zenodo.1214456) to assess texturing approaches. The image composition of the databases NCT-CRC-HE-100K and CRC-VAL-HE-7K is shown in Table I.

TABLE I. Database Composition

Class	Number of Images in NCT-CRC-HE-100K Database	Number of Images in CRC-VAL-HE-7K Database
adipose tissue	10,407	1,338
background (no tissue)	10,566	847
debris	10,512	339
lymphocytes	11,557	634
mucus	8,896	1,035
muscle	13,536	592
normal mucosa	8,763	741
stroma	10,446	421
tumor epithelium	14,317	1,233

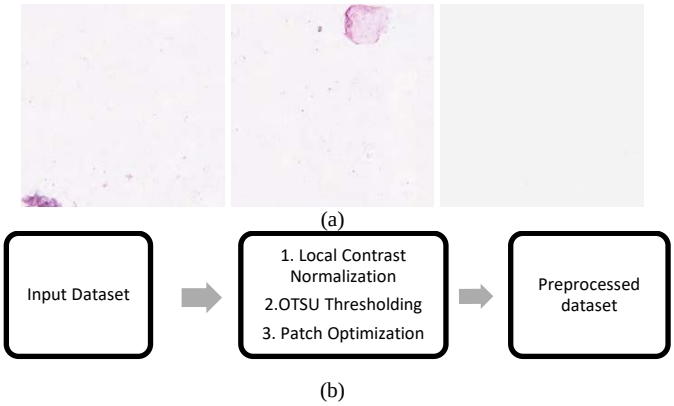

Fig. 1. Empty Patches in Database (b) Proposed Preprocessing Workflow.

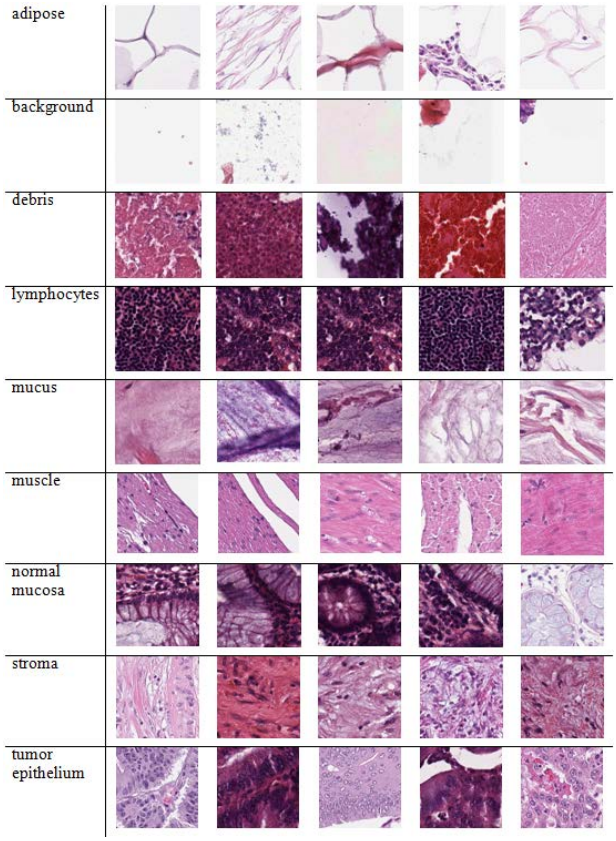

Fig. 2. Samples from the Kather-CRC- Database [12].

B. Preprocessing of Dataset

By removing the empty tissue patch from the dataset, extra computations have been avoided on the non-tissue regions of the slide. There are many different techniques to evaluate an image's contrast. In deep learning, the standard deviation of an image's pixels or a region of an image is commonly referred to as contrast in equation (1) and (2).

$$\sqrt{\frac{1}{3rc}\sum_{i=1}^{r}\sum_{j=1}^{c}\sum_{k=1}^{3}(X_{i,j,k}-\bar{X})^2} \quad (1)$$

where $\bar{X}$ is the mean intensity of the entire image:

$$\bar{X}=\frac{1}{3rc}\sum_{i=1}^{r}\sum_{j=1}^{c}\sum_{k=1}^{3}X_{i,j,k} \quad (2)$$

compute the LCN as proposed in [18] which is given in equation (3)

$$V_{i,j,k}=X_{i,j,k}-\sum_{i,p,q}w_{pq}x_{i,j+p.k+q} \quad (3)$$

Where $w_{pq}$is the Gaussian waiting window.

The RGB colour scheme of the low-resolution image was changed to LAB colour space before applying OTSU's threshold. After thresholding, binary morphological techniques were carried out to assist in the accurate patch extraction at small tissue regions and tissue borders. Fig. 1(a) shows few samples of empty patches available in the database and Fig. 1(b) shows the proposed preprocessing flow for preprocessing the database. Even after separating the tissue region there is a chance of extracting patches with no information. So, one more step of patch optimization has been added to discard empty patches as shown in Fig. 1(b).

C. CNN Architectures

Three of the most powerful fine-tuned CNN architectures, Alexnet, GoogLeNet, and Inception-v3 have been tested. Pre-trained models have been employed in this instance that was developed using the Kather-CRC-database [12].

D. Alexnet

The architecture is made up of eight layers: five convolutional layers and three fully connected layers. However, this is not what distinguishes AlexNet from other convolutional neural networks; rather, they are some of the characteristics that are employed. AlexNet uses Rectified Linear Units (ReLU) in place of the tanh function, which was referred as the industry standard. ReLU outperforms Tanh in terms of training velocity. A CNN utilizing ReLU was able to achieve a 25% error on the CIFAR-10 dataset six times quicker. CNNs frequently "pool" the outputs of neighboring neural groups without any overlap. However, after adding the overlapping, the error was reduced by roughly 0.5%, and it was shown that models with overlapping pooling are often more difficult to overfit. Overfitting was a serious concern for AlexNet.

E. GoogLeNet

The primary design of GoogLeNet [25] enhances computational capabilities inside the network model to encompass inception layers with the goal of minimizing complexity. By adding 1x1 convolutional layers to the network and using a different kernel, it not only enhances the depth but also the width of the architectural approach. In order to capture sparse correlation patterns, this lowers the number of computing levels

F. Inception-v3

The third iteration of the Inception networks family, which was initially introduced in [27], is known as Inception-v3 [34]. Inception block uses stacked 1x1 convolutions to reduce dimensionality, enabling fast computing and deeper networks. Unlike previous CNNs, which stacked kernel filter sizes sequentially, Inception architectures run several kernel filters with varying size on the same level. Making the networks larger rather than deeper is meant by this. The authors in [22,23] depicts the architecture of Inception-v3, which differs from the original Inception versions in a number of ways. These enhancements include propagating label information further down the network via an auxiliary classifier, factorized 7x7 convolutions, and label smoothing.

G. Fine-Tuning of Selected Models

Fine-tuning is a transfer learning concept in which information gained via training with one kind of difficulty is applied to training with another similar task or area [35]. The initial layers of deep learning algorithms are instructed to identify task-specific traits. The transfer learning phase is used

to remove few final layers of learnt network which can then be retrained with better task specified layers. Even if fine-tuned learning trials involve some learning, they nonetheless proceed far more quickly than learning from beginning [36]. Additionally, compared to models created from scratch, they are more accurate.

Data augmentation was used to fine-tune CNN Alexnet, Inceptionv3, GoogLeNet, and architecture using the Nct-Crc-He-100k and CRC-VAL-HE-7K datasets. The pretrained model has undergone the following adjustment.

1) The overfitting is greater if the size of the target data set is smaller and more comparable to the size of the training data set. The amount of overfitting that necessitates fine-tuning the data set for the pre-trained model is minimal if the target data set is bigger and comparable in size to the training data [37]. Therefore, a dropout layer has been added with probability 0.6 to the network to replace the final dropout layer, "pool5-drop 7x7 s1," which will randomly set certain features to zero.

2) Frequency can be modified based on the number of images allocated for training as follows.

$$Validation\ Frequency = \left\lfloor \frac{Number\ of\ Images}{Batch\ Size} \right\rfloor$$

3) The models were developed and then loaded with ImageNet pre-trained weights. As a result, a new fully-connected layer was developed in order to conduct the classification layer.

IV. Experimental Results

A. Experimental Setup

The main components of the hardware environment are an Radeon RX 550X video card and an Intel Core i7-85650 CPU with 16 GB of RAM. Matlab R2020a is the software environment for language programming on a Windows 10 computer.

B. Dataset

To evaluate the fine-tuned pretrained model, two databases have been used: CRC-VAL-HE-7K and NCT-CRC-HE-100K. The bigger dataset of 100,000 non-overlapping image patches, NCT-CRC-HE-100K, and the smaller dataset of 7180, CRC-VAL-HE-7K, were chosen for testing. The comparison criteria used are displayed in Tables II and III. A total of 40% of the images in each dataset were used as the training set, 20% as the validation set, and 40% as the testing set.

C. Discussion

In the area of machine learning for image processing, deep learning models have prevailed. The possibility to extend the study and application to the identification and categorization of tumor epithelium in high resolution images is presented by advancements in deep learning and image processing. However, the main problem with high quality images is training time.

TABLE II. Parameter Values Taken for Comparison (Nct-Crc-He-100kDatabase)

Fields	Size
Number of Classes	9
Dropout Probability	0.8 Vs pretrained models
Batch size	64
Epoch	15
Iterations	9360
Learning rate	$1e^{-05}$

TABLE III. Parameter Values Taken for Comparison (CRC-VAL-HE-7K Database)

Fields	Size
Number of Classes	9
Dropout Probability	0.4 Vs pretrained models
Batch size	64
Epoch	15
Iterations	660
Learning rate	$1e^{-05}$

TABLE IV. Training, Validation and Testing Accuracy of NCT-CRC-HE-100K Database

(Batch size = 64, Iterations = 9360, Learning rate = $1e^{-05}$,Epoch =15)					
Model	**Training Acc. (%)**	**Validation Acc. (%)**	**Training Loss**	**Testing Acc.(%)**	**Testing Loss**
Alexnet	95	95.03	0.42	94.5	0.39
GoogLeNet	95	94.08	0.38	94.3	0.29
InceptionV3	98	97.79	0.21	97.42	0.25

TABLE V. Training, Validation and Testing Accuracy of CRC-VAL-HE-7K Database

(Batch size = 64, Iterations = 660, Learning rate = $1e^{-05}$, Epoch =15)					
Model	**Training Acc. (%)**	**Validation Acc. (%)**	**Training Loss**	**Testing Acc.(%)**	**Testing Loss**
Alexnet	93	93.18	0.51	93.2	0.43
GoogLeNet	92	91.36	0.59	91.4	0.7
InceptionV3	89.4	89.57	0.71	89	0.73

The deep learning architectures are adjusted in accordance with Section 3.G's instructions. Fig. 3 to 7 displays the experiment's findings. The accuracy and dropout probability of deep learning models (Alexnet, GoogLeNet and Inceptionv3) are shown in Fig. 3 and 4. For the pretrained model the default dropout parameter is 0.5 and it has been adjusted to 0.4 (for small dataset) and 0.8 (for large dataset) which is shown in Fig. 3 and 4. Therefore over fitting issue is properly handled using the dropout parameter which results good in both training set and the validation set. As the validation frequency has been generalized based on the size of the database, the batch loss and validation loss are very less which is shown in the Fig. 5, 6 and 7. Based on the above adjustments, all the models' accuracy increased after 15 epochs.

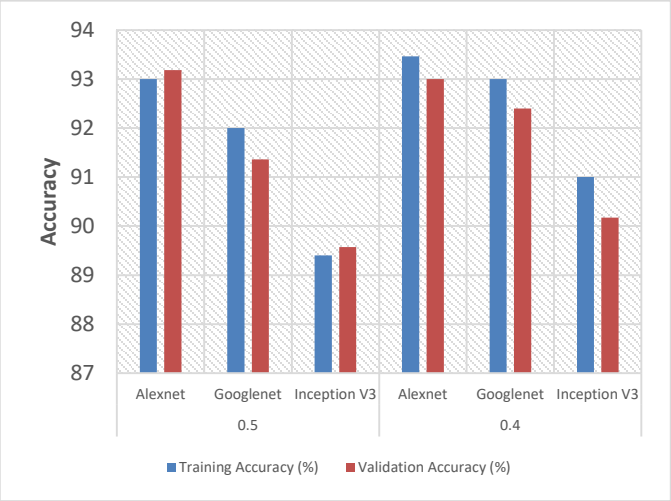

Fig. 3. Accuracy Comparison with and without Dropout Layer (CRC-VAL-HE-7K Database).

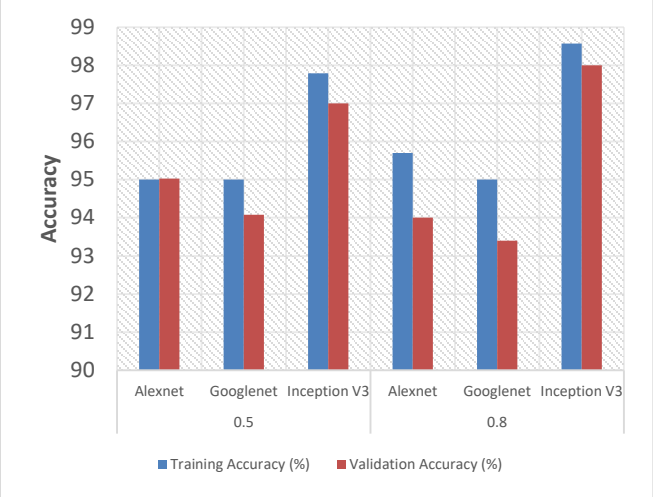

Fig. 4. Accuracy Comparison with and without Dropout Layer (NCT-CRC-HE-100K DATABASE).

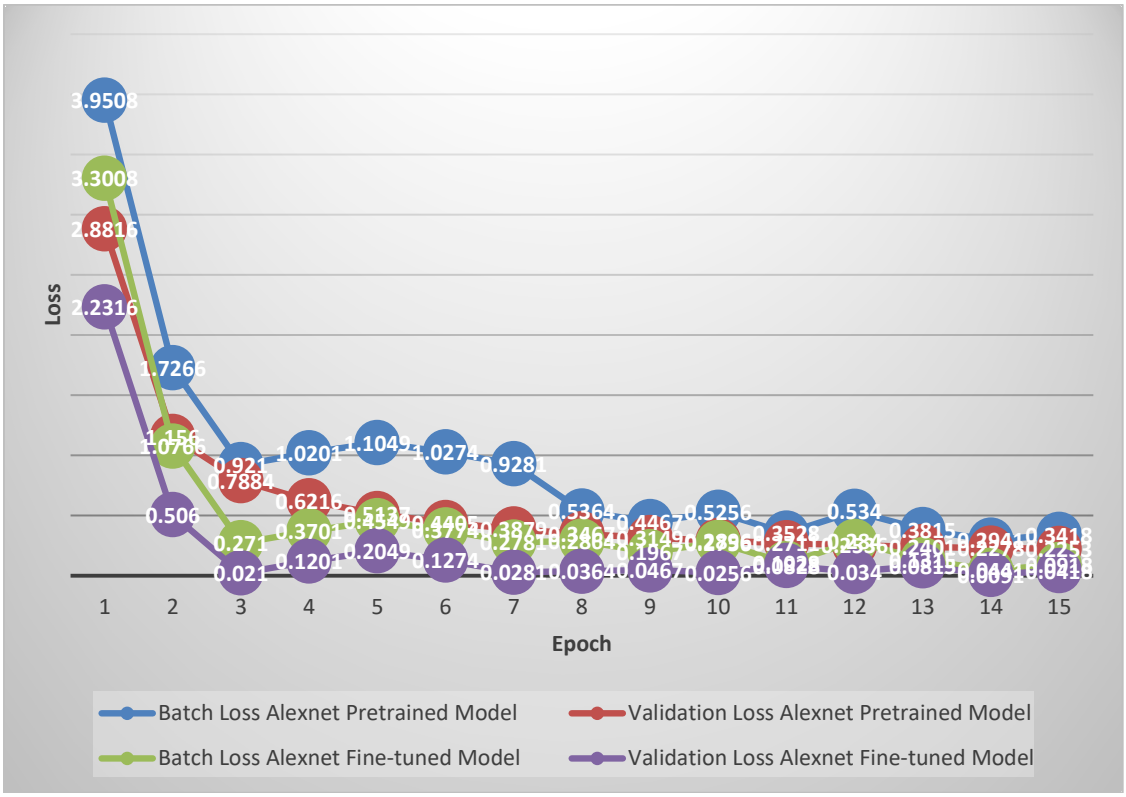

Fig. 5. Epoch Vs Batch Loss and Validation Loss of Alexnet.

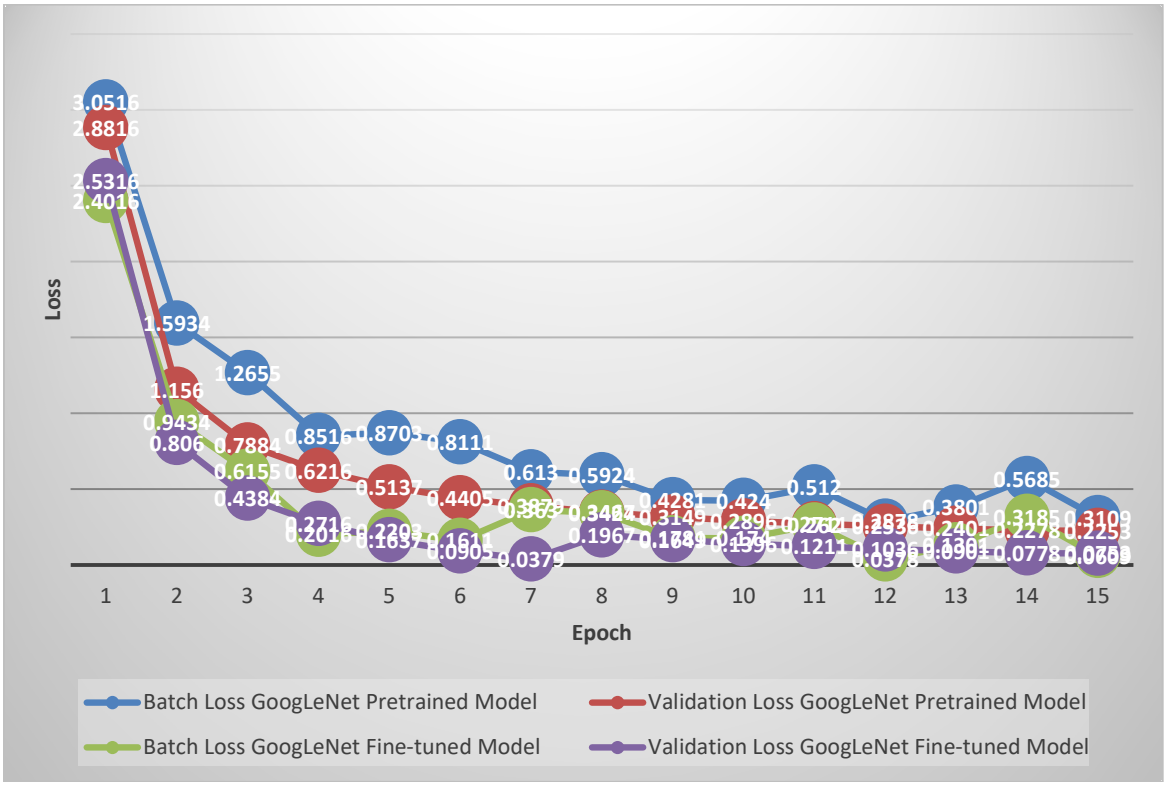

Fig. 6. Epoch Vs Batch Loss and Validation Loss of GoogLeNet.

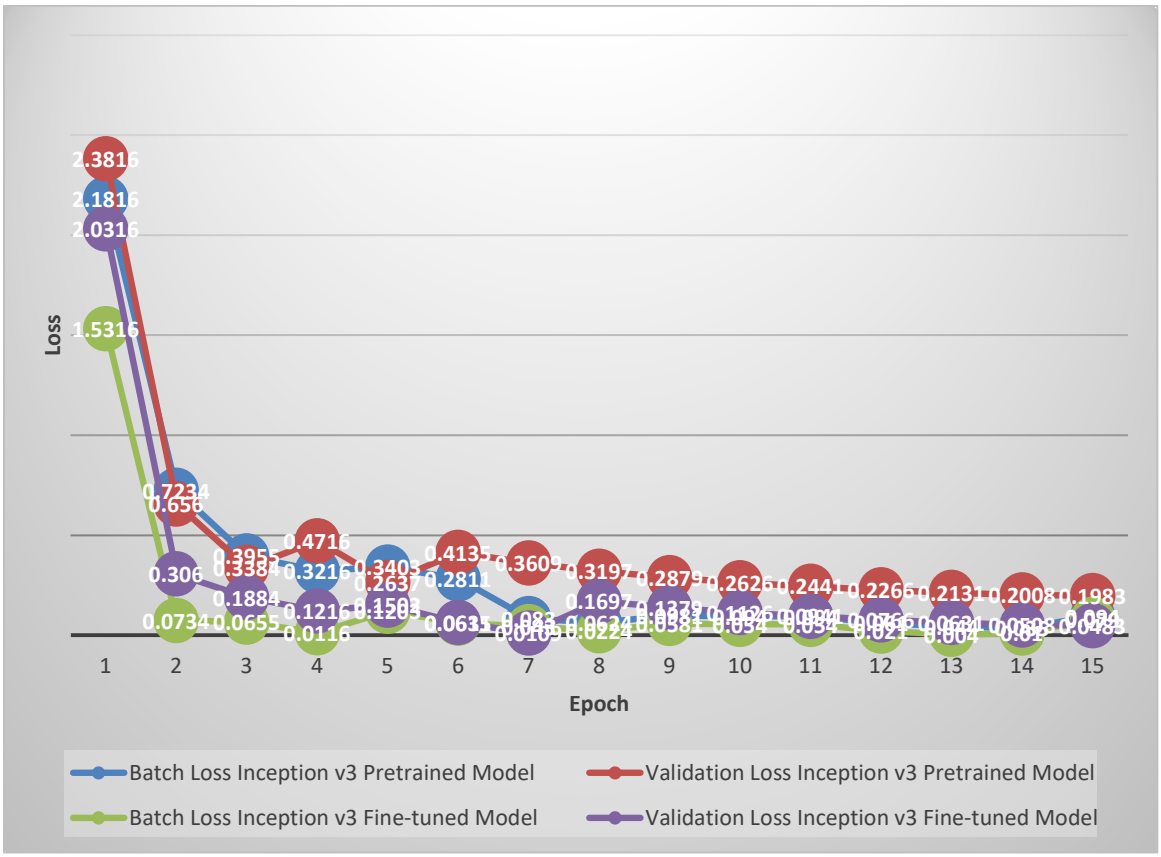

Fig. 7. Epoch Vs Batch Loss and Validation Loss of Inception v3.

TABLE VI. TISSUE AND TUMOR EPITHELIUM CLASSIFICATION ACCURACY USING PRETRAINED MODELS (CRC-VAL-HE-7K DATABASE)

Tissue Class	Alexnet	GoogLeNet	Inceptionv3
Adipose	97.8	97.6	94.23
Background	99.4	99.7	98.4
Debris	99.2	91.7	99
Lymphocytes	92.7	92.6	95.1
Mucus	94.6	92.7	85.4
Smooth Muscle	81	78.0	86.36
Normal Colon Mucosa	85.9	93.3	85.98
Stroma	84.7	88.2	90.26
Tumor epithelium	88.7	89.9	92.45

TABLE VII. TISSUE AND TUMOR EPITHELIUM CLASSIFICATION ACCURACY USING FINE-TUNED MODELS (CRC-VAL-HE-7K DATABASE)

Tissue Class	Alexnet	GoogLeNet	Inceptionv3
Adipose	98.5	98.1	95.73
Background	99.6	99.7	99.9
Debris	99.5	93.5	99.5
Lymphocytes	93.1	92.5	96.6
Mucus	95.2	93.4	86.9
Smooth Muscle	85.23	84.5	87.86
Normal Colon Mucosa	89.56	95.2	87.48
Stroma	90.21	91.78	92.76
Tumor epithelium	92.24	92.45	95.95

TABLE VIII. TISSUE AND TUMOR EPITHELIUM CLASSIFICATION ACCURACY USING PRETRAINED MODELS (NCT-CRC-HE-100K DATABASE)

Tissue Class	Alexnet	GoogLeNet	Inceptionv3
Adipose	97.5	98.31	99.61
Background	98.5	99.57	99.4
Debris	93.5	94.6	95.9
Lymphocytes	97.6	98.45	99.75
Mucus	95.4	96.21	97.51
Smooth Muscle	95.4	96.41	97.71
Normal Colon Mucosa	91.9	93.8	95.1
Stroma	88.4	91.3	92.6
Tumor epithelium	94.9	95.8	97.1

TABLE IX. TISSUE AND TUMOR EPITHELIUM CLASSIFICATION ACCURACY USING FINE-TUNED MODELS (NCT-CRC-HE-100K DATABASE)

Tissue Class	Alexnet	GoogLeNet	Inceptionv3
Adipose	98.4	99.09	99.5
Background	99.4	99.35	99.29
Debris	94.4	95.38	96.79
Lymphocytes	98.5	99.23	99.64
Mucus	96.3	96.99	98.4
Smooth Muscle	96.3	97.19	98.6
Normal Colon Mucosa	92.8	94.58	95.99
Stroma	89.3	92.08	93.49
Tumor epithelium	95.8	96.58	97.99

TABLE X. TRAINING TIME FOR FINE-TUNED MODELS

	Training Time CRC-VAL-HE-7K Database in Seconds		Training Time CRC-VAL-HE-7K Database in Seconds	
Models	No preprocessing	Proposed preprocessing	No preprocessing	Proposed preprocessing
Alexnet	3060	2564	307380	256897
GoogLeNet	8520	6295	83880	51520
Inception V3	41520	11265	110735	92545

The validation accuracy of the proposed finetuned Alexnet is better when compared to the validation accuracy proposed in [38]. The later achieved 91.8% accuracy with 25 epoch whereas this work achieved 93.18 % (Table V) and 95.03 (Table IV) in 15 epochs using the same database. The author in [39] claimed, that the network they developed, SCDNet, achieved an accuracy of 96.91% which is 4% more than the pretrained inception v3 model. The proposed fine-tuned inceptionv3 model achieves 97.79% accuracy which is better when compared to SCDNet. Additionally, as shown in Fig. 5 to 7, good accuracy results were obtained for all the chosen models even after the 30th training iteration with much reduced batch and validation loss.

GoogLeNet and Inceptionv3 models regularly outperform Alexnet among the three models chosen. Tables VI, VII, VIII, and IX shows the accuracy of nine tissue classes mentioned in Table I. As shown in Tables VI, VII, VIII, and IX, the accuracy of the tumor epithelium classification is higher in inceptionv3. Table X shows the training time required to execute the finetuned models based on the experimental setup. As indicated in Table X, training time has been reduced by at least 30% using the suggested preprocessing workflow. Overall, Alexnet fared badly, having the least accuracy and having the largest batch and validation loss, whereas finetuned inceptionv3 performed well, having the highest accuracy and the lowest batch and validation loss.

V. CONCLUSION

A workflow has been suggested to preprocess the dataset in this article. Additionally, the most advanced deep convolutional neural network for classifying tissues and tumor epithelium is being tuned and evaluated. The architectures under consideration are Inceptionv3, GoogLeNet, and Alexnet. According to the experiment, Inceptionv3 tends to provide a cogent accuracy increase with increasing epochs, without showing any signs of overfitting or performance degradation. Additionally, Inceptionv3 performs better in classification exhibitions with few parameters and fair processing time. Inceptionv3 outperforms the other architectures with a test accuracy score of 97.42% for the 15 epoch. Thus, Inceptionv3

is a promising design for the goal of identifying tumor epithelium. The proposed parameters can be extended with other pretrained models and the performance can be compared with the parameters F1-score, AUC, Recall and Precision. Also, a new generalized Deep CNN model can be designed which satisfies the proposed adjustment parameters.

REFERENCES

[1] Farahani, N.; Parwani, A.V.; Pantanowitz, L. Whole slide imaging in pathology: Advantages, limitations, and emerging perspectives. Pathol. Lab. Med. Int. 2015, 7, 4321.

[2] M. Zeeshan, B. Salam, Q. S. B. Khalid, S. Alam, and R. Sayani, ''Diagnostic accuracy of digital mammography in the detection of breast cancer,'' J. Cureus, vol. 10, no. 4, p. e2448, Apr. 2018, doi: 10.7759/cureus.2448.

[3] M. N. Gurcan, L. E. Boucheron, A. Can, A. Madabhushi, N. M. Rajpoot, and B. Yener, ''Histopathological image analysis: A review,'' IEEE Rev. Biomed. Eng., vol. 2, pp. 147–171, 2009, doi: 10.1109/RBME.2009.2034865.

[4] J. Hipp, A. Fernandez, C. Compton, and U. Balis, ''Why a pathology image should not be considered as a radiology image,'' J. Pathol. Informat., vol. 2, no. 1, p. 26, 2011, doi: 10.4103/2153-3539.82051.

[5] M. D. Pickles, P. Gibbs, A. Hubbard, A. Rahman, J. Wieczorek, and L. W. Turnbull, ''Comparison of 3.0T magnetic resonance imaging and X-ray mammography in the measurement of ductal carcinoma in situ: A comparison with histopathology,'' Eur. J. Radiol., vol. 84, no. 4, pp. 603–610, Apr. 2015, doi: 10.1016/j.ejrad.2014.12.016.

[6] Pantanowitz, L.; Sharma, A.; Carter, A.B.; Kurc, T.; Sussman, A.; Saltz, J. Twenty years of digital pathology: An overview of the road travelled, what is on the horizon, and the emergence of vendor-neutral archives. J. Pathol. Inform. 2018, 9, 40.

[7] Egeblad, M.; Nakasone, E.S.; Werb, Z. Tumors as organs: Complex tissues that interface with the entire organism. Dev. Cell 2010, 18, 884–901.

[8] Huijbers, A.; Tollenaar, R.; Pelt, G.W.; Zeestraten, E.C.M.; Dutton, S.; McConkey, C.C.; Domingo, E.; Smit, V.; Midgley, R.; Warren, B.F. The proportion of tumor-stroma as a strong prognosticator for stage II and III colon cancer patients: Validation in the VICTOR trial. Ann. Oncol. 2013, 24, 179–185.

[9] Marusyk, A.; Almendro, V.; Polyak, K. Intra-tumor heterogeneity: A looking glass for cancer? Nat. Rev. Cancer 2012, 12, 323–334.

[10] Bray, F.; Ferlay, J.; Soerjomataram, I.; Siegel, R.L.; Torre, L.A.; Jemal, A. Global cancer statistics 2018: GLOBOCAN estimates of incidence and mortality worldwide for 36 cancers in 185 countries. CA Cancer J. Clin. 2018, 68, 394–424.

[11] 7. Sirinukunwattana, K.; Snead, D.; Epstein, D.; Aftab, Z.; Mujeeb, I.; Tsang, Y.W.; Cree, I.; Rajpoot, N. Novel digital signatures of tissue phenotypes for predicting distant metastasis in colorectal cancer. Sci. Rep. 2018, 8, 1–13.

[12] Kather, Jakob Nikolas, et al. "Predicting survival from colorectal cancer histology slides using deep learning: A retrospective multicenter study." PLoS medicine 16.1 (2019): e1002730..

[13] 9. Nearchou, I.P.; Soutar, D.A.; Ueno, H.; Harrison, D.J.; Arandjelovic, O.; Caie, P.D. A comparison of methods for studying the tumor microenvironment's spatial heterogeneity in digital pathology specimens. J. Pathol. Inform. 2021, 12, 6.

[14] Sigirci, I. Onur, Abdulkadir Albayrak, and Gokhan Bilgin. "Detection of mitotic cells in breast cancer histopathological images using deep versus handcrafted features." Multimedia Tools and Applications 81.10 (2022): 13179-13202.

[15] Huynh BQ, Li H, and Giger ML. Digital mammographic tumor classification using transfer learning from deep convolutional neural networks. J. Med. Imaging 3:34501, 2016.

[16] Tran H, Phan H, Kumar A, Kim J, and Feng D. Transfer Learning of a Convolutional Neural Network for Hep-2 Cell Image Classification 2012:1208–1211, 2016.

[17] Zhang R, Zheng Y, Mak TWC, Yu R, Wong SH, Lau JYW, and Poon CCY. Automatic Detection and Classification of Colorectal Polyps by Transferring Low-Level CNN Features from Nonmedical Domain. IEEE J. Biomed. Heal. Informatics 21:41–47, 2017.

[18] Shin HC, Roth HR, Gao M, Lu L, Xu Z, Nogues I, Yao J, Mollura D, and Summers RM. Deep Convolutional Neural Networks for Computer-Aided Detection: CNN Architectures, Dataset Characteristics and Transfer Learning. IEEE Trans. Med. Imaging 35:1285–1298, 2016

[19] Pan Y, Huang W, Lin Z, Zhu W, Zhou J, Wong J, and Ding Z. Brain Tumor Grading Based on Neural Network s and C onvolutional Neural Network s. Eng. Med. Biol. Soc. (EMBC), 2015 37th Annu. Int. Conf. IEEE 699–702, 2015.doi:10.1109/EMBC.2015.7318458

[20] Kather, J.N.; Weis, C.A.; Bianconi, F.; Melchers, S.M.; Schad, L.R.; Gaiser, T.; Marx, A.; Zöllner, F.G. Multi-class texture analysis in colorectal cancer histology. Sci. Rep. 2016, 6, 27988

[21] Kothari, S.; Phan, J.H.; Young, A.N.; Wang, M.D. Histological image classification using biologically interpretable shape-based features. BMC Med. Imaging 2013, 13, 9.

[22] Javed, S.; Mahmood, A.; Fraz, M.M.; Koohbanani, N.A.; Benes, K.; Tsang, Y.W.; Hewitt, K.; Epstein, D.; Snead, D.; Rajpoot, N. Cellular community detection for tissue phenotyping in colorectal cancer histology images. Med. Image Anal. 2020, 63, 101696.

[23] Bejnordi, B.E.; Mullooly, M.; Pfeiffer, R.M.; Fan, S.; Vacek, P.M.; Weaver, D.L.; Herschorn, S.; Brinton, L.A.; van Ginneken, B.; Karssemeijer, N. Using deep convolutional neural networks to identify and classify tumor-associated stroma in diagnostic breast biopsies. Mod. Pathol. 2018, 31, 1502–1512.

[24] Nanni, L.; Brahnam, S.; Ghidoni, S.; Lumini, A. Bioimage classification with handcrafted and learned features. IEEE/ACM Trans. Comput. Biol. Bioinform. 2018, 16, 874–885.

[25] Bougourzi, F.; Dornaika, F.; Mokrani, K.; Taleb-Ahmed, A.; Ruichek, Y. Fusion Transformed Deep and Shallow features (FTDS) for Image-Based Facial Expression Recognition. Expert Syst. Appl. 2020, 156, 113459.

[26] Wang, S.; Yang, D.M.; Rong, R.; Zhan, X.; Fujimoto, J.; Liu, H.; Minna, J.; Wistuba, I.I.; Xie, Y.; Xiao, G. Artificial intelligence in lung cancer pathology image analysis. Cancers 2019, 11, 1673.

[27] Ouahabi, A.; Taleb-Ahmed, A. Deep learning for real-time semantic segmentation: Application in ultrasound imaging. Pattern Recognit. Lett. 2021, 144, 2–34.

[28] Cascianelli, S.; Bello-Cerezo, R.; Bianconi, F.; Fravolini, M.L.; Belal, M.; Palumbo, B.; Kather, J.N. Dimensionality reduction strategies for cnn-based classification of histopathological images. In Proceedings of the International Conference on Intelligent Interactive Multimedia Systems and Services, Gold Coast, Australia, 20–22 May 2018; pp. 21–30.

[29] Kather, J.N.; Krisam, J.; Charoentong, P.; Luedde, T.; Herpel, E.; Weis, C.A.; Gaiser, T.; Marx, A.; Valous, N.A.; Ferber, D. Predicting survival from colorectal cancer histology slides using deep learning: A retrospective multicenter study. PLoS Med. 2019, 16, e1002730.

[30] Simonyan, K.; Zisserman, A. Very deep convolutional networks for large-scale image recognition. arXiv 2014, arXiv:1409.1556.

[31] Krizhevsky, A.; Sutskever, I.; Hinton, G.E. Imagenet classification with deep convolutional neural networks. Commun. ACM 2017, 60, 84–90.

[32] Iandola, F.N.; Han, S.; Moskewicz, M.W.; Ashraf, K.; Dally, W.J.; Keutzer, K. SqueezeNet: AlexNet-level accuracy with 50x fewer parameters and

[33] Szegedy, C.; Liu, W.; Jia, Y.; Sermanet, P.; Reed, S.; Anguelov, D.; Erhan, D.; Vanhoucke, V.; Rabinovich, A. Going deeper with convolutions. In Proceedings of the IEEE Conference on Computer Vision and Pattern Recognition, Boston, MA, USA, 7–12 June 2015; pp. 1–9.

[34] He, K.; Zhang, X.; Ren, S.; Sun, J. Deep residual learning for image recognition. In Proceedings of the IEEE Conference on Computer Vision and Pattern Recognition, Las Vegas, NV, USA, 27–30 June 2016; pp. 770–778.

[35] Pan, S.J., Fellow, Q.Y., 2009. A Survey on Transfer Learning, pp. 1–15.

[36] Mohanty, S. P., D. P. Hughes, and M. Salathé. "Using deep learning for image-based plant disease detection 7, 1–10." (2016).

[37] Senan, Ebrahim Mohammed, et al. "Classification of histopathological images for early detection of breast cancer using deep learning." Journal of Applied Science and Engineering 24.3 (2021): 323-329.

[38] Izzaty, Al Mira Khonsa, et al. "Multiclass classification of histology on colorectal cancer using deep learning." Commun. Math. Biol. Neurosci. 2022 (2022)

[39] Naeem, Ahmad, et al. "SCDNet: A Deep Learning-Based Framework for the Multiclassification of Skin Cancer Using Dermoscopy Images." Sensors 22.15 (2022): 5652.